AGU PUBLICATIONS

JGR

Journal of Geophysical Research: Space Physics

RESEARCH ARTICLE

10.1002/2015JA021787

Key Points:

- An ionospheric data assimilation system with GPS-TEC has been developed in this study
- This data assimilation system is evaluated by disturbed ionosphere during the geomagnetic storm
- The shorter assimilation time interval can greatly improve the capability of model forecast

Correspondence to:
C. H. Chen,
koichi@mail.ncku.edu.tw

Citation:
Chen, C. H., C. H. Lin, T. Matsuo, W. H. Chen, I. T. Lee, J. Y. Liu, J. T. Lin, and C. T. Hsu (2016), Ionospheric data assimilation with thermosphere-ionosphere-electrodynamics general circulation model and GPS-TEC during geomagnetic storm conditions, *J. Geophys. Res. Space Physics*, *121*, 5708–5722, doi:10.1002/2015JA021787.

Received 10 AUG 2015
Accepted 24 MAY 2016
Accepted article online 27 MAY 2016
Published online 17 JUN 2016

Ionospheric data assimilation with thermosphere-ionosphere-electrodynamics general circulation model and GPS-TEC during geomagnetic storm conditions

C. H. Chen[1], C. H. Lin[1], T. Matsuo[2,3], W. H. Chen[1], I. T. Lee[4], J. Y. Liu[5,6], J. T. Lin[1], and C. T. Hsu[5]

[1]Department of Earth Sciences, National Cheng Kung University, Tainan, Taiwan, [2]Cooperative Institute for Research in Environmental Sciences, University of Colorado Boulder, Boulder, Colorado, USA, [3]Space Weather Prediction Center, National Oceanic and Atmospheric Administration, Boulder, Colorado, USA, [4]Central Weather Bureau, Taipei, Taiwan, [5]Institute of Space Science, National Central University, Chung-Li, Taiwan, [6]Center for Space and Remote Sensing Research, National Central University, Chung-Li, Taiwan

Abstract The main purpose of this paper is to investigate the effects of rapid assimilation-forecast cycling on the performance of ionospheric data assimilation during geomagnetic storm conditions. An ensemble Kalman filter software developed by the National Center for Atmospheric Research (NCAR), called Data Assimilation Research Testbed, is applied to assimilate ground-based GPS total electron content (TEC) observations into a theoretical numerical model of the thermosphere and ionosphere (NCAR thermosphere-ionosphere-electrodynamics general circulation model) during the 26 September 2011 geomagnetic storm period. Effects of various assimilation-forecast cycle lengths: 60, 30, and 10 min on the ionospheric forecast are examined by using the global root-mean-squared observation-minus-forecast (OmF) TEC residuals. Substantial reduction in the global OmF for the 10 min assimilation-forecast cycling suggests that a rapid cycling ionospheric data assimilation system can greatly improve the quality of the model forecast during geomagnetic storm conditions. Furthermore, updating the thermospheric state variables in the coupled thermosphere-ionosphere forecast model in the assimilation step is an important factor in improving the trajectory of model forecasting. The shorter assimilation-forecast cycling (10 min in this paper) helps to restrain unrealistic model error growth during the forecast step due to the imbalance among model state variables resulting from an inadequate state update, which in turn leads to a greater forecast accuracy.

1. Introduction

Compared with earlier ionospheric models, recent empirical and physics-based models have substantially improved their ability to reproduce observed features to the level of tracking the ionospheric "climate" well [e.g., *Lu et al*., 2008]. However, there models are still unable to predict the ionospheric "weather," especially during geomagnetic storms when dynamical time scales become short, because physical mechanisms remained inadequately described in models [*Sojka et al*., 2007].

Recently, there are a growing number of studies [*Hajj et al*., 2004; *Pi et al*., 2004; *Wang et al*., 2004; *Schunk et al*., 2004, 2005; *Scherliess et al*., 2004, 2006; *Thompson et al*., 2006; *Khattatov et al*., 2004, 2005; *Matsuo and Araujo-Pradere*, 2011; *Lee et al*., 2012, 2013; *Hsu et al*., 2014] suggesting that data assimilation could improve the accuracy of theoretical numerical models of the ionosphere. Ionospheric data assimilation during geomagnetic storms is however still challenging, primarily due to the rapid changes of forcings, including electric fields, auroral particle precipitations, and Joule heating. Improving the accuracy of storm time ionospheric nowcasting and forecasting is important and is the focus of this paper. For example, *Solomentsev et al*. [2014] developed an ionospheric assimilation system to perform electron density nowcasting during geomagnetic storm conditions, achieving great improvements in the total electron content (TEC) specification at high latitudes with 2–4 total electron content unit, 1 TECU = 10^{16} el m^{-2} (TECU) accuracy. Another assimilation model developed by *Datta-Barua et al*. [2013] was used to estimate the storm time $E \times B$ drift, one of the important forcings from the electron density observations. *Chartier et al*. [2016] assimilated the ground-based TEC observations into a coupled thermosphere-ionosphere model during a major storm of *Kp* 7–8 and evaluated their model capabilities/performances for storm time short-term forecasting. Using synthetically generated observations, *Chartier et al*. [2013] and *Hsu et al*. [2014] have examined the impact of initializing the

thermospheric states on long-term ionospheric forecasting. Their results suggest that a longer electron density forecasting performance can be achieved by accurately initializing thermospheric state variables, especially the neutral composition, in a coupled thermosphere-ionosphere model.

In this paper, we use the ensemble Kalman filter (EnKF) to assimilate global GPS total electron content (TEC observations into a theoretical numerical model (thermosphere-ionosphere-electrodynamics general circulation model (TIE-GCM)) developed by the National Center for Atmospheric Research (NCAR) in order to adjust the model states by observations. This ionospheric data assimilation system includes updating of the thermospheric state variables, as in previous studies using the same system [*Matsuo and Araujo-Pradere*, 2011; *Lee et al*., 2012, 2013; *Hsu et al*., 2014; *Chartier et al*., 2016]. This system is employed in the current study for nowcasting and forecasting ionospheric electron densities during a geomagnetic storm that occurred on 26 September 2011. In order to track the rapid storm time variations, we conduct assimilation experiments with different assimilation-forecast cycle lengths and evaluate the impact of rapid cycling on the ionospheric nowcast/forecast during this geomagnetic storm event. During this storm, the *Kp* index reaches its maximum value of 6+ between 15:00 and 20:00 UT, and the *Dst* index reaches its maximum of −103 nT around 23:00 UT during the main phase, which is followed by a typical recovery phase. The ionospheric effect of this geomagnetic storm event has been reported by previous studies [*Baumgardner et al*., 2013; *Thomas et al*., 2013; *Wang et al*., 2013].

2. Methodology

An EnKF data assimilation system built with the Data Assimilation Research Testbed (DART) community software, developed and maintained by the NCAR Data Assimilation Research Section, is employed in the present study to combine the TIE-GCM and ground-based GPS-TEC observations. Details of the DART are described by *Anderson et al*. [2009].

The TIE-GCM is a three-dimensional global model of the thermosphere-ionosphere which solves the momentum, energy, and continuity equations for neutral and plasma species as well as the electrodynamical processes for the coupling of neutral and plasma species. The solar UV and EUV fluxes in this model are parameterized according to the solar $F_{10.7}$ daily index. At high latitudes, the ion convention pattern is parameterized by the cross-tail potential and the interplanetary magnetic field using the Heelis model [*Heelis et al*., 1982]. At low and middle latitudes, the electric fields are calculated by the Richmond model with the assumption of equal potential magnetic field [*Richmond et al*., 1992]. The lower boundary of the model is at ~97 km in altitude with the upper boundary varying between 500 and 800 km depending on the solar activity [*Roble et al*., 1988; *Richmond et al*., 1992]. The model applies a spherical geographic coordinate system with a default horizontal resolution of 5°×5° in longitude and latitude and a vertical resolution of a half-scale height.

The TEC observations are derived from the ground-based GPS receivers, along slant line-of-sight radio path between GPS satellites and receivers. As the GPS network can provide a continuous global monitoring of the ionosphere, the two-dimensional TEC map in the longitude-latitude plane is useful for studying global ionosphere dynamics [*Wilson et al*., 1992; *Sardon et al*., 1994; *Liu et al*., 1996]. After removing the GPS satellites' and receiver's biases [cf. *Liu et al*., 1996], a nominal observational error of GPS-TEC is set to a random value between 2 and 4 TECU (1 TECU = 10^{16} electron/m^2) with the uniform distribution. The observational error might come from inadequate receiver bias estimation and/or multipath effect [cf. *Bhuiyan*, 2011].

In this study, we use data from 2119 ground-based GPS receivers provided by the International Global Navigation Satellite Systems Service (IGS) https://igscb.jpl.nasa.gov/components/data.html) and calculate the vertical TEC from the slant TEC by using the slant function of *Liu et al*. [1996]. Then we further calculate the median vertical TEC value within 1°×1° in longitude and latitude. The GPS-TEC observations are assimilated to adjust the TEC values predicted by the TIE-GCM. Note that TIE-GCM has an upper boundary located around 500–800 km in altitude, while GPS satellites are at a significantly higher altitude (around ~20,200 km). In this paper, the electron density (*Ne*) above the upper boundary in the model is calculated as

$$N_{e,h} = N_{e,h'} \exp\left(-\frac{h-h'}{H}\right), \tag{1}$$

where h is the altitude above the upper boundary (h' in the equation) and H is the scale height of electron density. Using this approximation, we can obtain the electron density up to the GPS altitude (around ~20,200 km) and

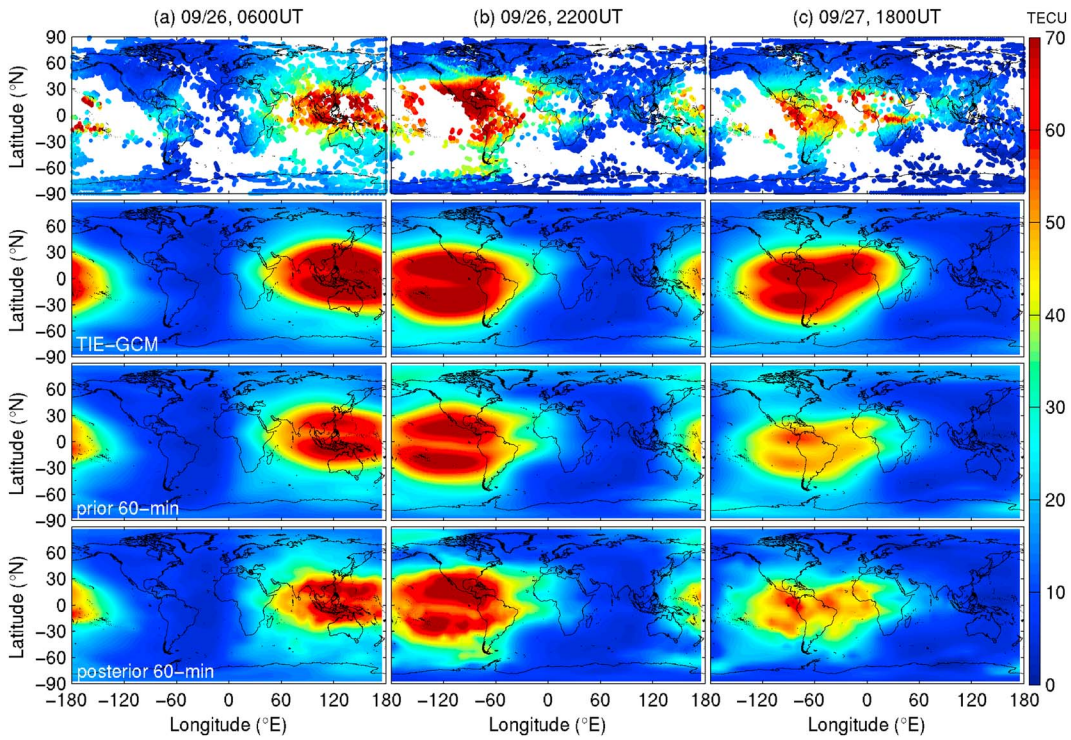

Figure 1. Global TEC map at (a) 06:00 UT on 26 September, (b) 22:00 UT on 26 September, and (c) 18:00 UT on 27 September. (top to bottom rows)TThe ground-based (first row) GPS-TEC observations, (second row) TIE-GCM modeled TEC with no dada assimilation (referred to as TIE-GCM in the legend henceforth), (third row) prior TEC of data assimilation, and (fourth row) posterior TEC of data assimilation, respectively. The unit of TEC is TECU (=10^{16} electron/m^2).

then calculate its integrated density in altitude to obtain the vertical TEC value. It is noted that the diffusive equilibrium assumption of the extended electron density given by equation (1) may introduce additional model uncertainty during the magnetic storm period.

In this study, the unobserved state variables (neutral temperature, atomic and molecular oxygen mixing ratios (O, O_2), neutral zonal wind (U), neutral meridional wind (V), atomic oxygen ion density (OP)) as well as *Ne* are included in the state vector of the DART/TIE-GCM data assimilation system. Note that the summation of O, O_2 and N_2 mixing ratios is 1 in the TIE-GCM model. Therefore, the adjustment of O and O_2 implicitly adjusts N_2 in this assimilation system. The half width of localization radius is set equal to around 1000 km in the horizontal direction, and the vertical localization function is not employed in this assimilation system. Following the work by *Lee et al*. [2012], the ensemble number is set to 90, and the ensemble simulations are initialized by perturbing solar $F_{10.7}$ and *Kp* indexes via centered Gaussian distributions. The standard deviation of $F_{10.7}$ distribution is $20\times10^{-22}\,\mathrm{Wm^{-2}Hz^{-1}}$ with the mean value of $269\times10^{-22}\,\mathrm{Wm^{-2}Hz^{-1}}$ [*Lee et al*., 2012]. The daily average *Kp* index on 26 September, 3+ with ±1 in the unit of *Kp*, is used to estimate the hemispheric power and cross-tail potential [*Boyle et al*., 1997; *Zhang and Paxton*, 2008]. Note that the width of *Kp* distribution is twice that of *Lee et al*. [2012] for the geomagnetic storm event. Furthermore, instead of employing the realistic variation of *Kp* index in this study, the constant *Kp* index (3+) with the spread of ±1 is employed to test the forecast performance of the assimilation system when the true storm time *Kp* variations is not known.

2.1. Storm Time Ionospheric Assimilation Results

Figure 1 illustrates the ionospheric data assimilation results during the geomagnetic storm event on 26 September 2011. In this case, GPS-TEC observations are assimilated every hour. In Figure 1 (top to bottom), the ground-based GPS-TEC observations (observed TEC), the mean TEC from an ensemble of TIE-GCM simulations without assimilation (modeled TEC, referred to as "TIE-GCM" in the figure henceforth), the mean TEC before assimilation (prior TEC), and the mean TEC after assimilation (posterior TEC) are shown. Note that the prior and posterior TEC indicates the mean value of 90-member ensemble TECs. Figure 1a presents the TEC

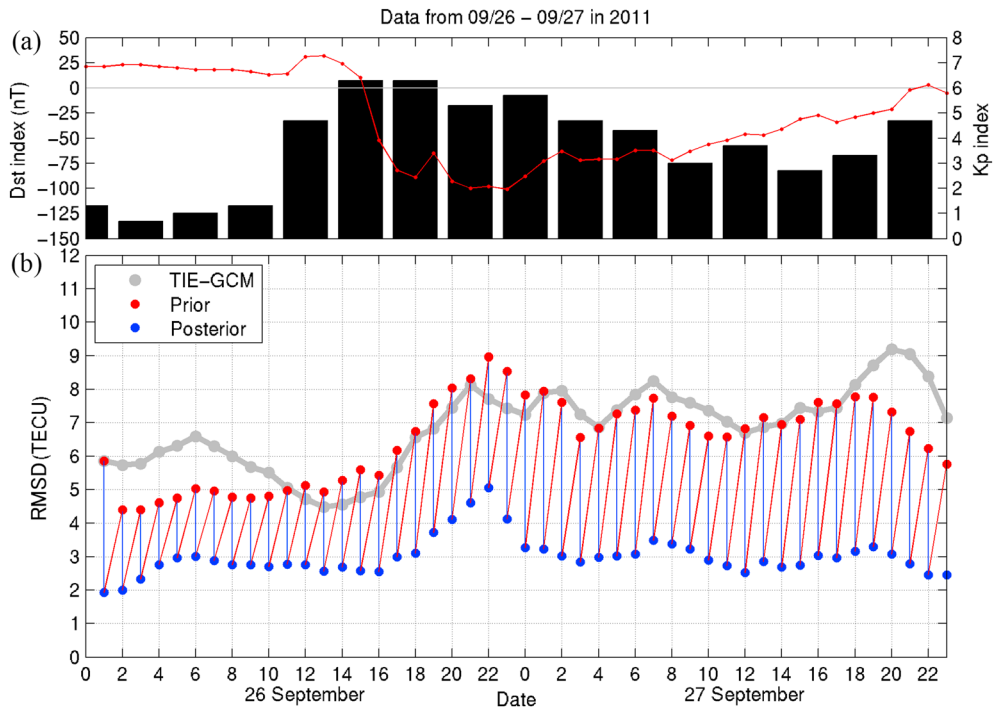

Figure 2. Time evolutions of (a) *Dst* index (red dotted line), *Kp* index (black bar), and (b) RMSD of data assimilation with the 60 min cycle. The gray line in Figure 2b indicates the TIE-GCM model control run with no data assimilation. The red and blue lines indicate the RMSD before and after the data assimilation, respectively.

maps at 06:00 UT on 26 September 2011 (day of year is 269), which is the time when the ionospheric electron densities had not yet been affected by the geomagnetic storm. Compared with the observed TEC, it can be seen that the TEC values are overestimated by the TIE-GCM (second panel). But this feature is corrected after data assimilation (bottom). Not only the TEC values but also the shapes of the equatorial ionization anomaly (EIA) on both the two hemispheres become similar to the observed TEC after the process of data assimilation.

Figure 1b is the global TEC distribution map at 22:00 UT. At this time, the ionospheric electron density was affected by the geomagnetic storm. It shows positive storm features of the enhanced TEC values in the EIA region. The assimilation results, prior/posterior TEC (Figure 1b, third and fourth panels), show a latitudinally separated EIA structure, while the modeled TEC shows a closer EIA structure. It is also interesting that a plume structure appears in the observed TEC map around the northern part of North America and extends to higher latitudes from the northern EIA region. Although this storm enhanced density (SED) [*Foster et al.*, 2002] structure is not reproduced by the TIE-GCM, it appears after assimilating ground-based GPS-TEC observations (posterior TEC). Figure 1c shows the global TEC distribution map during the storm recovery phase at 18:00 UT on 27 September 2011 (see *Dst* and *Kp* indexes in Figure 2a). Compared with the TIE-GCM TEC, the prior and posterior TEC features generally agree better with the observed TEC.

To assess impacts of data assimilation of ground-based TEC observations, the global root-mean-square difference (RMSD) against the observed TEC is computed as

$$\mathrm{RMSD} = \sqrt{\frac{\sum_{i=1}^{N}\left(\mathrm{TEC}_i^{obs} - \mathrm{TEC}_i'\right)^2}{N}} \tag{2}$$

in which N is the total number of observed TEC (TEC^{obs} in the equation). TEC′ is either modeled, prior, or posterior TEC, which is interpolated to the locations of TEC observation. The smaller value of RMSD indicates the TEC has a value closer to the observation.

The RMSDs of TIE-GCM simulations with or without data assimilation during the geomagnetic storm event are presented in Figure 2b. The assessment of RMSD shows that the ionospheric data assimilation system can

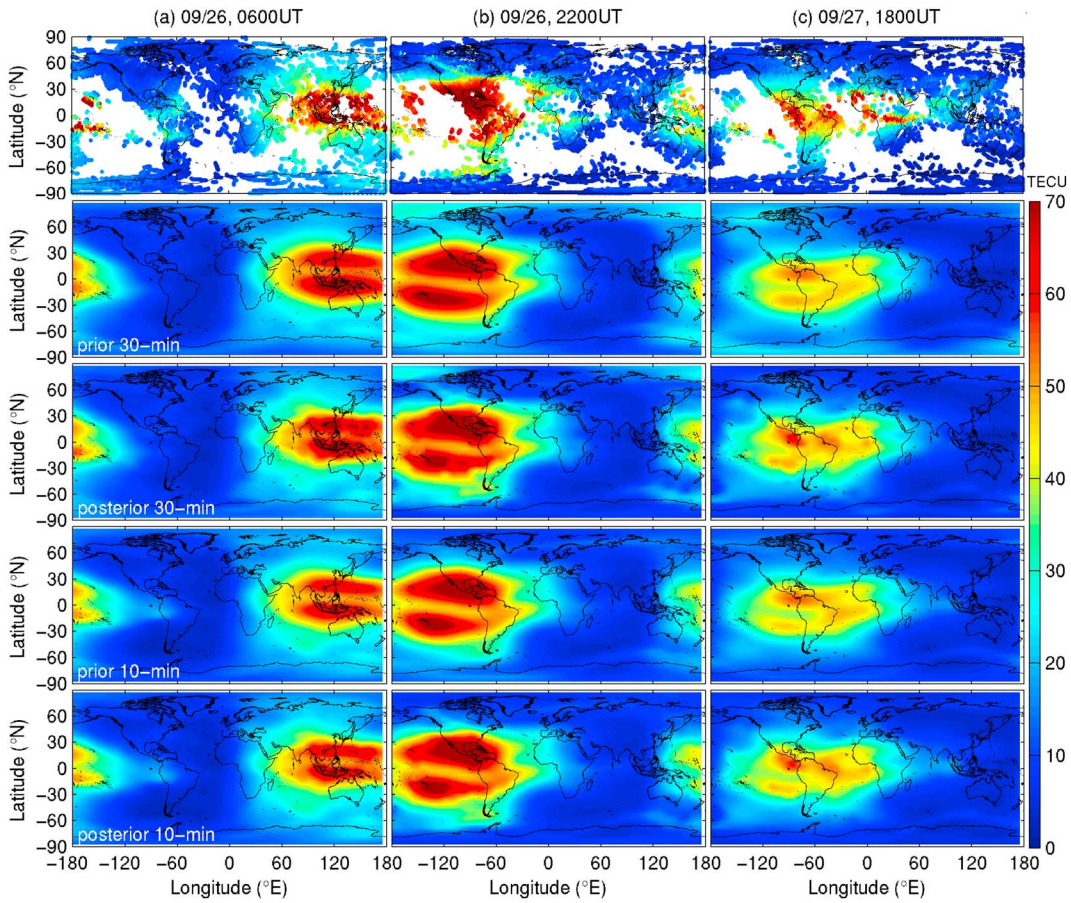

Figure 3. The similar format as Figure 1 but for the 30 and 10 min cycling cases. (first row) The observed GPS-TEC, which is the same data with Figure 1 (top). (second and third rows) The prior TEC and posterior TEC of the data assimilation with 30 min cycle, respectively. (fourth and fifth rows) The prior TEC and posterior TEC of the data assimilation with 10 min cycle, respectively.

adjust the modeled TEC toward the GPS-TEC observations as suggested by the smaller posterior TEC RMSD shown in blue dots in comparison to the prior TEC RMSE in red dots. In addition, the prior RMSD exhibits a great improvement over the TIE-GCM RMSD during quiet time conditions (before 10:00 UT). However, it is clearly seen that the prior RMSD rises up to the magnitude that is even larger than the TIE-GCM RMSD during both the main and recovery phases of geomagnetic storm. The prior TEC can be seen as the short-term (1 h in this case) forecast result by the TIE-GCM model using initial conditions provided by the posterior data assimilation analysis. This indicates that this ionospheric data assimilation system could successfully improve ionospheric forecasting during geomagnetically quiet conditions but has considerable inaccuracies during geomagnetic storm conditions.

During geomagnetic storms, the ionospheric electron density changes rapidly, especially during the initial and main phases where the penetrating magnetospheric electric fields vary rapidly. The present ionospheric data assimilation system with 60 min assimilation-forecast cycling may not be able to swiftly adapt to ionospheric storm effects with time scales shorter than 60 min. Therefore, we shorten the assimilation-forecast cycles length to 30 and 10 min with the same geophysical conditions (e.g., $F_{10.7}$ index, hemispheric power, and cross-tail potential) as in the case of 60 min cycling. The resulting global TEC distribution maps are shown in Figure 3. The first row is the observed TEC. The second and third rows in Figure 3 display the 30 min cycle assimilation results (prior TEC and posterior TEC), and the fourth and fifth rows are for the case with 10 min cycling. Both 30 and 10 min cycle assimilation results clearly show considerable difference from the TIE-GCM TEC (Figure 1, second row). The prior and posterior TECs more closely resemble the TEC observations. In the case of the 30 min cycle length, the feature of two extended EIA crests has a similar pattern with results with the 60 min cycle length. Additionally, a larger TEC region around the Arctic Ocean appears at 22:00 UT on 26

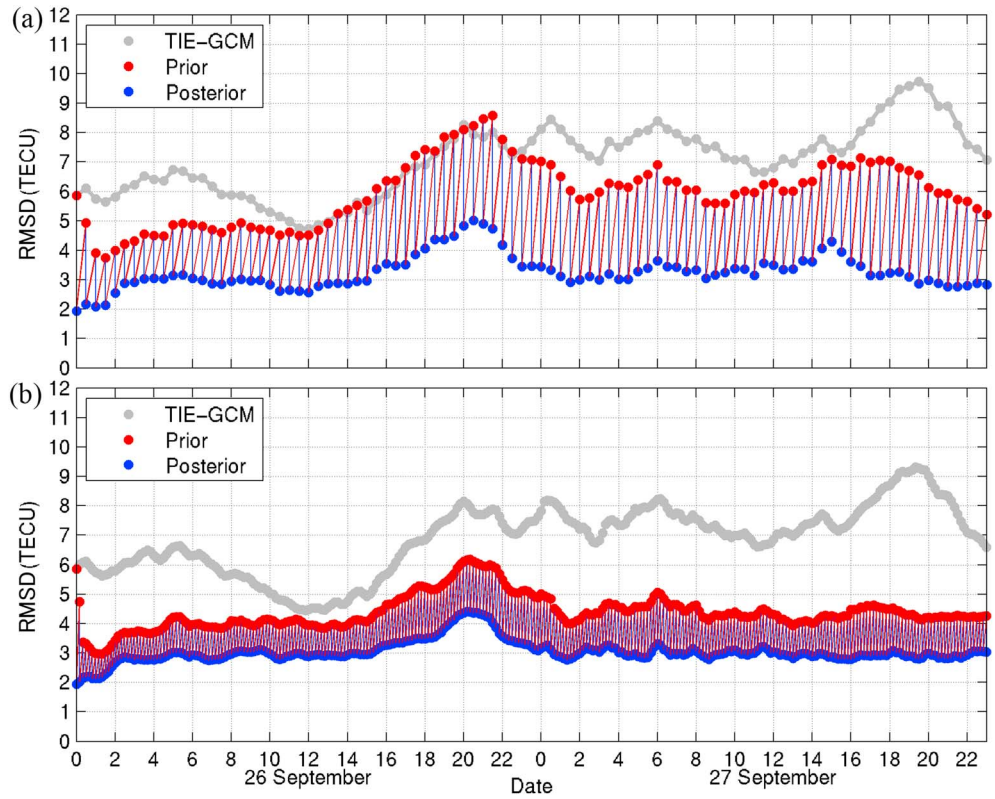

Figure 4. The same format as Figure 2b but for the case of (a) 30 min and (b) 10 min assimilated cycles.

September and 18:00 UT on 27 September in results with 30 min cycling. The similar feature is also seen in the case of the 60 min cycle length (Figure 1b, third and fourth panels). However, this high TEC feature is unrealistic because of its absence in the observed TECs (top rows of Figures 1 and 3, top rows). In contrast, the assimilation results obtained with 10 min cycling capture observed features faithfully. The above-mentioned unrealistic TEC region around the Arctic Ocean does not appear in this case. The SED density structure more clearly extends to the polar region at 22:00 UT on 26 September, as shown in Figure 3b (bottom). However, the prior TEC (Figure 3b, fourth panel) indicates that it is still difficult to forecast the formation of SED even with a 10 min assimilation-forecast cycle.

To further quantify the improvement of the ionospheric data assimilation system shown in Figure 3, Figures 4a and 4b show the time evolution of RMSDs in the case of 30 and 10 min cycling, respectively. Compared with the 60 min cycling case, 30 min cycling yields a smaller model error growth during the forecast steps as indicated by smaller prior RMSDs during 00:00 UT–14:00 UT on 27 September, the storm recovery phase. However, during the storm main phase (12:00 UT–23:00 UT on 26 September), the benefit of shorter assimilation-forecast cycling is limited for the 30 min cycling case. It shows almost the same RMSD value as that of TIE-GCM with no assimilation. When the cycling length shortens to 10 min, as a result, the prior RMSD shown in Figure 4b becomes smaller than the TIE-GCM control case, resulting in a great improvement of assimilation analysis quality, compared with the 60 min and 30 min cycling cases.

The 10 min forecasts initialized by data assimilation with the different cycle lengths are further compared and shown in Figure 5. Results show the forecast TEC of 10 min cycling agrees better with the observations in both amplitude and shape than that of 60 and 30 min cycles, especially during the storm main phase period (Figure 5b). In Figure 5b, the global prior RMSDs of the 10 min cycling case is around 4.22 TECU (bottom) which is lower than that of the standalone TIE-GCM run (~7.23 TECU, second panel), the 60 min assimilation cycle (~7.42 TECU, third panel), and the 30 min assimilation cycle (~6.64 TECU, fourth panel). These results further support that the ionosphere assimilation with shorter assimilation-forecast cycling, 10 min in this paper, could considerably improve the quality of EnKF data assimilation analysis during geomagnetic storms.

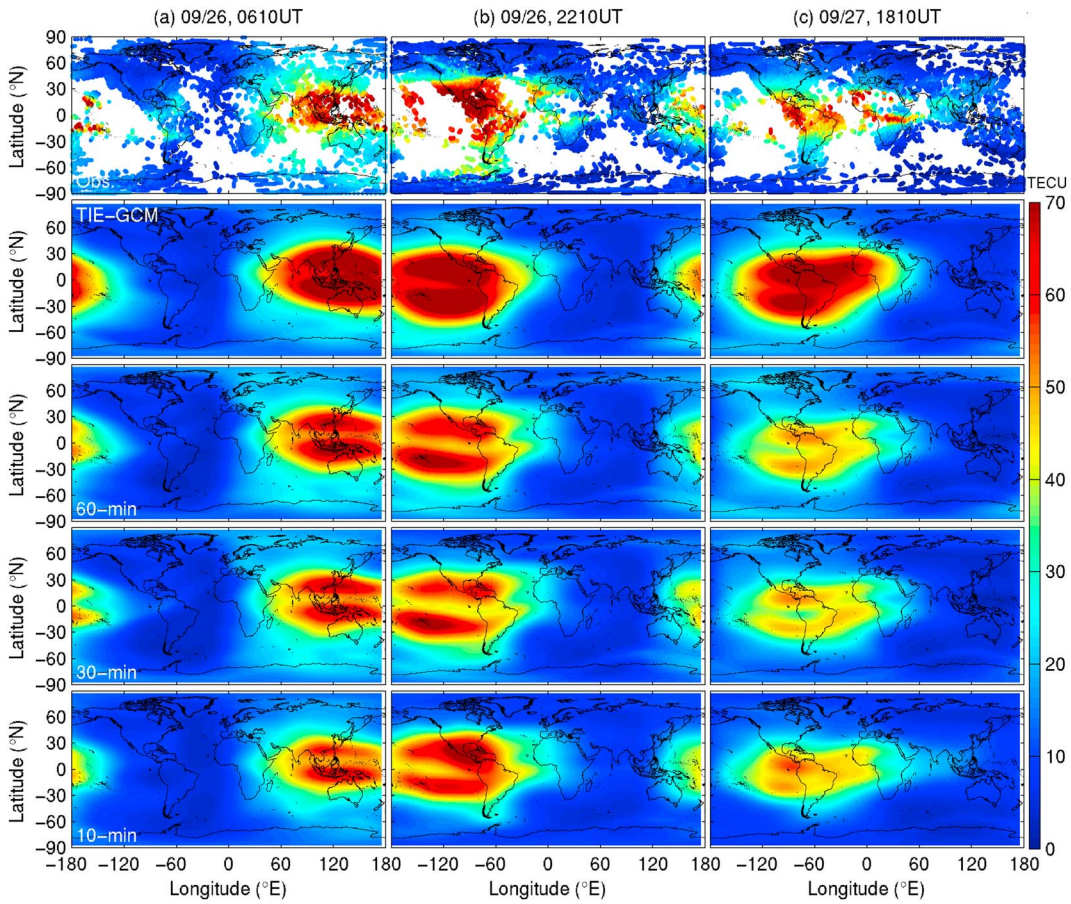

Figure 5. The 10 min forecast of global TEC map at (a) 06:10 UT on 26 September, (b) 22:10 UT on 26 September, (c) and 18:10 UT on 27 September. (first row to last row) The ground-based GPS-TEC observations, TIE-GCM modeled TEC without dada assimilation (referred to as TIE-GCM in the legend henceforth), prior TEC by 60 min assimilation cycle, prior TEC by 30 min assimilation cycle, and prior TEC by 10 min assimilation cycle, respectively. The unit of TEC is TECU (=10^{16} electron/m^2).

3. Discussions

As demonstrated in Figure 1, the observed TEC enhances significantly (positive storm effect) during the main phase of the geomagnetic storm at 22:00 UT on 26 September and reduces (negative storm effect) during the storm recovery phase at 18:00 UT on 27 September. The TIE-GCM simulation (with no data assimilation) in Figure 1 shows high TEC values during the entire assimilation period. After assimilating the ground-based GPS-TEC observations, the prior and posterior TECs elevate to higher values during the storm main phase and then reduce to the nominal values during the storm recovery phase. This feature is similar to the observed TEC. The assessment of RMSDs shown in Figure 2b suggests that the modeled TECs are well adjusted by the observations during the quiet time conditions but that the adjustment is inadequate during the storm time conditions. To examine the impact of EnKF parameters for ionospheric forecasting during storm time, shorter assimilation-forecast cycling intervals have been used in the subsequent assimilation experiments. Results (Figures 2b and 4) show that the assimilation with a 30 min cycling interval can reduce the model error growth in the forecast step during the recovery phase of geomagnetic storm, bringing down the prior RMSD in comparison to the 60 min cycling case. The 10 min cycling case further leads to a greater improvement, especially for the prior RMSD, during the storm main phase. The comparative experiments presented in this paper demonstrate that the EnKF assimilation system with shorter assimilation-forecast cycling perform better for ionospheric specification and forecasting during the geomagnetic storm period.

In order to investigate the main physical mechanisms that lead to better short-term forecasting (i.e., smaller RMSDs for the prior state) by adopting faster assimilation-forecast cycling, roles of the neutral temperature, meridional/zonal neutral winds, and $\Sigma[O]/[N_2]$ ratio are considered. Note that the neutral composition

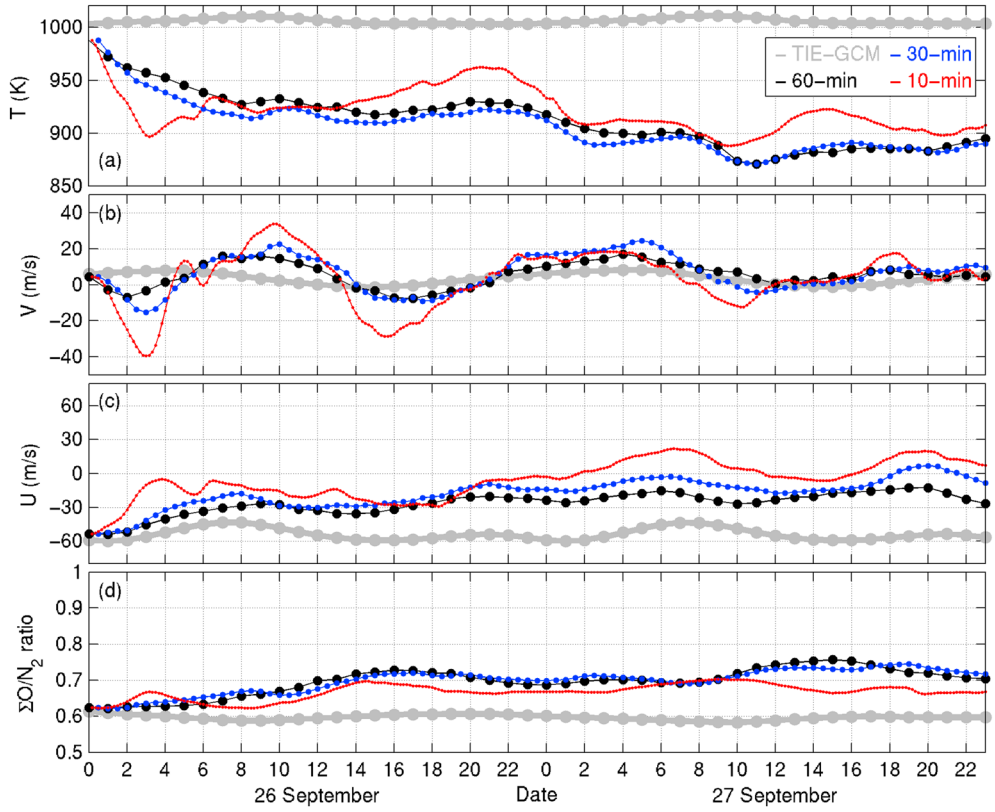

Figure 6. Time evolution of (a) global averaged neutral temperature, (b) meridional neutral wind, (c) zonal neutral wind, and (d) $\Sigma[O]/[N_2]$ ratio in the prior stage of assimilation. The gray line indicates the TIE-GCM with no data assimilation. The black, blue, and red lines denote the assimilated results in the case of 60 min, 30 min, and 10 min cycles, respectively.

$\Sigma[O]/[N_2]$ ratio is calculated by taking the ratio of [O] column density to $[N_2]$ column density above an altitude where the $[N_2]$ column density is 10^{17} cm^{-2} [cf. *Strickland et al.*, 1995]. This definition is commonly adopted for comparison with satellite observations of ultraviolet airglow, as with the Thermosphere, Ionosphere, Mesosphere Energetics and Dynamics/Global Ultraviolet Imager (TIMED-GUVI) data. Figure 6 illustrates the time evolution of global mean neutral temperature (*T*), meridional neutral wind (*V*), zonal neutral wind (*U*), and $\Sigma[O]/[N_2]$ ratio during the prior stage of data assimilation at the end of short-term forecasting. It is clearly seen that the assimilation processes reduce the neutral temperature and increases the zonal wind $\Sigma[O]/[N_2]$ ratio as well as the variation of meridional wind. It is interesting to note that the cases with 60 and 30 min cycling have similar values and variations, except for the zonal wind velocity during the storm recovery phase. This suggests that the prior RMSD improvement during the storm recovery phase from the case with 60 min cycling (Figure 2b) and to be 30 min cycling case (Figure 4a) might originate from the changes in zonal neutral wind. Furthermore, the data assimilation with 10 min cycling shows a substantial difference from that with 60 and 30 min cycling. One of the possible reasons for the significant prior RMSD improvement of about 2 TECU (i.e., 5.5 TECU down from 7.5 TECU) during the storm main phase (Figure 4b) might be a better representation of $\Sigma[O]/[N_2]$ ratio variation compared with the 60 and 30 min cycling cases. At higher latitudes, upwelling of neutral atmosphere results a decrease in the $\Sigma[O]/[N_2]$ ratio, while at low latitudes, downwelling leads to an increase of the $\Sigma[O]/[N_2]$ ratio [*Fuller-Rowell et al.*, 1998]. Therefore, temperature changes are often associated with global $\Sigma[O]/[N_2]$ ratio disturbances. These characteristics were seen by the GUVI O/N_2 ratio observation and the model simulation for example during the geomagnetic storm event in November 2003 [*Meier et al.*, 2005]. At midlatitudes, meridional winds can also lift or lower the ionospheric layer along the magnetic fields into the atomic oxygen-rich atmosphere (greater O/N_2 ratio) or molecular rich atmosphere (lesser O/N_2 ratio). Since the neutral composition change substantially affect the ionosphere through its strong control of the loss process of atomic oxygen ion O+, it is important to represent the composition

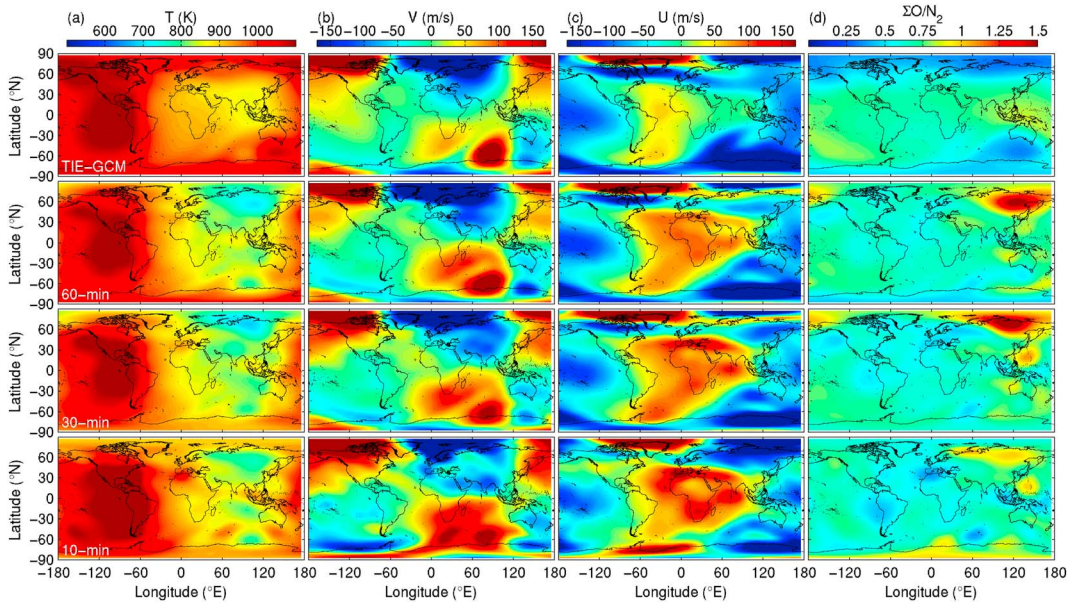

Figure 7. Global maps of (a) neutral temperature, (b) meridional neutral wind, (c) zonal neutral wind, and (d) $\Sigma[O]/[N_2]$ ratio in the prior stage of assimilation at 22:00 UT on 26 September. (first to last rows) The TIE-GCM model run with no data assimilation, 60, 30, and 10 min cycles, respectively. The positive values of meridional neutral wind (*V*) and zonal neutral wind (*U*) are indicated the northward and eastward winds, respectively.

changes that are consistent with other model states in the forecast step. The fast change of ionospheric electron density along with changes in the thermospheric states during the storm main phase is unlikely to be tracked with longer assimilation-forecast cycling, such as 60 and 30 min. The EnKF assimilation system with a shorter cycling interval, such as 10 min in this study, could correct the imbalance in the model state rapidly and then yield better model initial conditions to further improve the accuracy of ionospheric forecasting.

Reproduction of the SED [cf. *Foster et al*., 2002; *Coster et al*., 2007] is also a noteworthy assimilation result. The SED is known for featuring a plume of electron density that is carried sunward and poleward by subauroral polarization streamers and electric field and eastward prompt penetration electric field, respectively [*Foster et al*., 2002]. The feature primarily appears around the afternoon/dusk sector at middle latitudes during the geomagnetic storm period. The appearance of SED during the same geomagnetic storm on 26 September 2011 was also reported by *Thomas et al*. [2013] using Super Dual Auroral Radar Network and GPS-TEC data. In the present study, the SED plume feature that is absent in the TIE-GCM simulation (Figure 1b, second panel) is successfully reproduced over North America by assimilating the GPS-TEC observations (Figure 1b, fourth panel). The SED feature is also reproduced in the cases of shorter assimilation-forecast cycling, such as 30 and 10 min (Figure 3b, third and fifth panels). For the 10 min cycle, the conjugate SED feature in the southern hemisphere is also present in the posterior plot (Figure 3b, fifth panel). A similar conjugate SED feature had been reported by *Foster and Rideout* [2007]. These results further suggest that an ionospheric data assimilation system with rapid assimilation-forecast cycling successfully reproduces the storm time electron density structure changes.

For the cases of 60 and 30 min cycling, there are a few regions showing unrealistic TEC enhancement that do not appear in the TEC observation or the assimilation-free TIE-GCM simulation. As shown in Figures 1b and 3b, during the storm main phase, a larger TEC value appears around the Arctic Ocean after the data assimilation with 60 and 30 min cycling, while the observation and TIE-GCM model do not show this kind of high-TEC region. This unrealistic TEC region does not appear in the case of 10 min assimilation-forecast cycle, as shown in Figure 3b (fifth panel). In order to explore mechanisms causing the larger TEC value, global distribution maps of neutral temperature and meridional/zonal neutral winds at a constant pressure surface (the global height range of 220~239 km with the average height of ~229 km in this simulation), as well as the $\Sigma[O]/[N_2]$ ratio, at assimilation prior stage at 22:00 UT on 26 September are examined. It can be seen in Figure 7 that around the Arctic Ocean region, the TIE-GCM $\Sigma[O]/[N_2]$ ratio is enhanced from 0.25 to around 0.75–1 by the

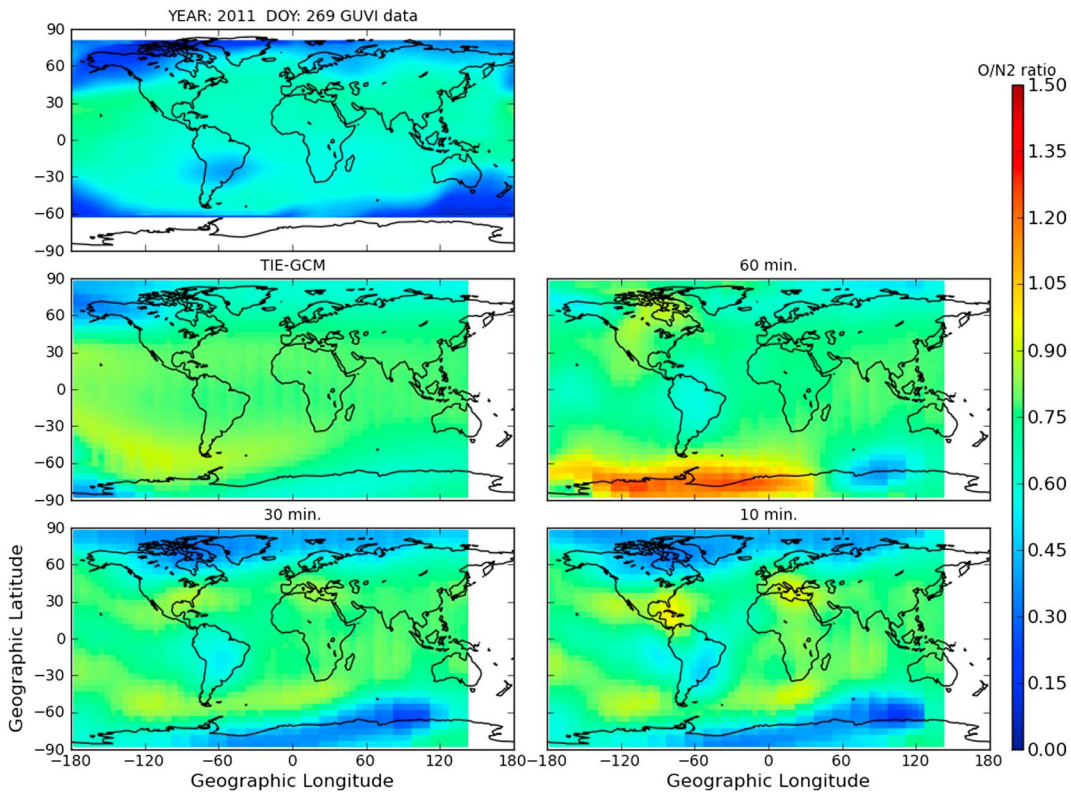

Figure 8. Global maps of O/N_2 ratio observed by (top left) TIMED-GUVI satellite, (middle left) TIE-GCM without data assimilation, (top right) 60, (bottom left) 30, and (bottom right) 10 min assimilation cycle at 09:00 LT on 26 September 2011.

ionospheric data assimilation system with different cycling intervals. It is worthwhile to note that the $\Sigma[O]/[N_2]$ ratio enhancement is smaller in the case of 10 min cycling compared with other cycling intervals. The overestimation of $\Sigma[O]/[N_2]$ ratio may be a cause of the high-TEC region in the Arctic Ocean region, and this unrealistic TEC structure can be restrained by the data assimilation with a shorter cycling interval. However, previous studies [e.g.,*Burns et al.*, 1995] have shown that during geomagnetic storms, the $[O]/[N_2]$ ratio typically increase at low-to-middle latitudes while decreasing at high latitudes. The enhanced $\Sigma[O]/[N_2]$ ratio at high latitude and reduced $\Sigma[O]/[N_2]$ ratio at low/middle latitudes by data assimilation (Figure 7d) contradict to the earlier study. Figure 8 shows the O/N_2 ratio observation by TIMED-GUVI satellite at 09:00 LT on 26 September as well as the calculated $\Sigma[O]/[N_2]$ without data assimilation and with assimilation using different cycling intervals. The TIMED-GUVI O/N_2 ratio shows a large decrease at high latitudes during the 26 September storm event, which is contrary to the assimilation results during the geomagnetic storm. The disagreement is magnified for the 60 min cycling case but is largely mitigated for the shorter assimilation-forecast cycling cases (30 and 10 min). In addition to a difference in the O/N_2 variations discussed above, the neutral winds show larger deviations from the control TIE-GCM run for the 10 min cycling case in comparison to the 30 and 60 min cycling cases (Figures 6 and 7).

To further evaluate the effects of dynamically unbalanced neutral state variables in the forecast model on the assimilation analysis, assimilation experiments in wihch only the ionospheric variables (electron density and O^+ density) are updated are further performed for the same geomagnetic storm event. Figure 9 illustrates the global TEC maps obtained 60 and 30 min assimilation-forecast cycling. Results clearly show the great agreements of TEC values with the observations, especially for the posterior results. Furthermore, the unrealistic TECs disappear in this case. The time evolution of global RMSDs in the cases of 60, 30, and 10 min assimilation-forecast cycling is further presented in Figure 10. It is clearly seen that the prior RMSDs have different features from those in Figures 2b and 4. For the entire period of the storm, especially during the main phase, the RMSDs shown in Figure 10 present improvements in comparison with those of assimilation experiment with neutral state variables included the EnKF state vector (Figures 2b and 4). Although the assimilations with

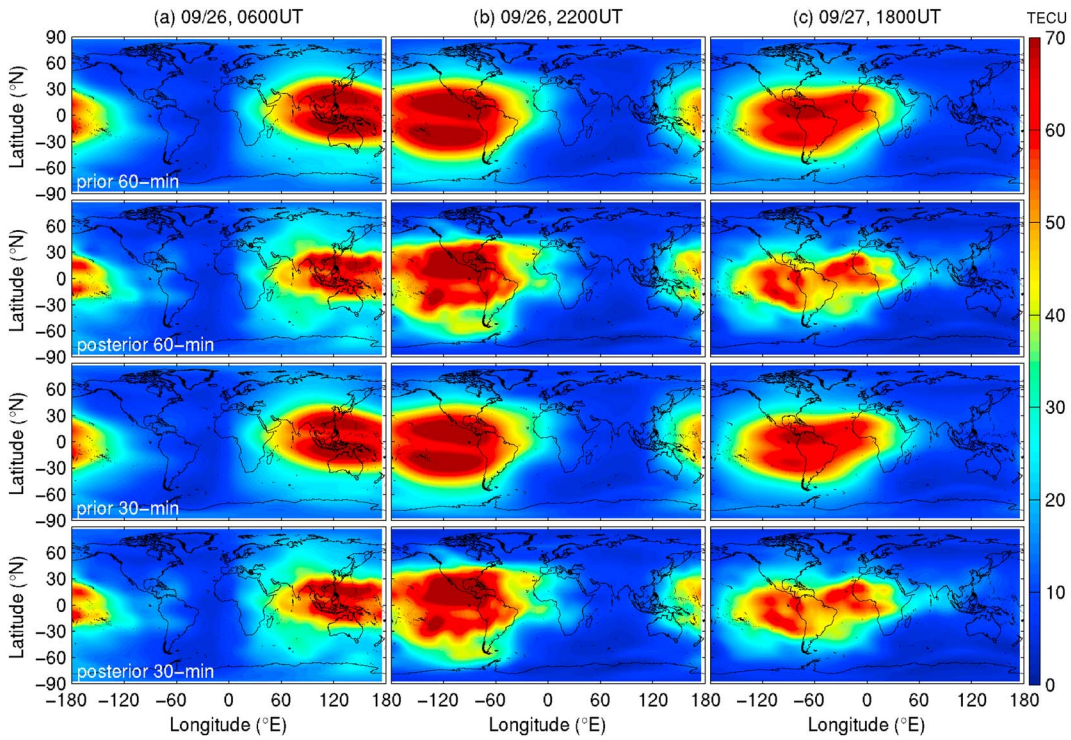

Figure 9. Global TEC map by the assimilation model with only the ionospheric variables at (a) 06:00 UT on 26 September, (b) 22:00 UT on 26 September, and (c) 18:00 UT on 27 September. The first and second rows are the prior TEC and posterior TEC of the data assimilation with 60 min cycle, respectively. The third and fourth rows are the prior TEC and posterior TEC of the data assimilation with 30 min cycle, respectively.

updating only ionospheric variables result in a better fit to the TEC observations, the weakness of such an assimilation system does not affect thermosphere-ionosphere dynamics as suggested by the fact that the prior and posterior results generally follow the forecast model trajectory. The TIE-GCM RMSDs and prior RMSDs (Figure 10) show very similar variation pattern at all times. In the assimilations updating both thermospheric and ionospheric stave variables (Figures 2b and 4), this similarity has been reduced after updating the neutral state variables in the forecast model, especially for the 10 min cycling case during the storm recovery phase. These results indicate that updating neutral states is the key to allowing GPS-TEC data to affect the forecast model dynamics. It is important to use shorter cycling intervals, 10 min for this study, in order to prevent unbalanced neutral states to cause a large model error growth during the forecast step. Unbalanced neutral states may partly be due to the limited spread of the TIE-GCM ensemble. The spread of *Kp* index associated with the 90-member ensemble roughly ranges from 2+ to 4+. In reality, the *Kp* index reaches its maximum value of 6+ during the storm main phase, exceeding the range of ensemble spread. It means that the ensemble-based covariance is not able to adequately represent the relationship between the GPS-TEC observations and the state variables.

To verify this hypothesis, an additional assimilation experiment is conducted. Realistic storm time *Kp* variations is used as the mean with a standard-deviation of ±1 to initialize the TIE-GCM ensemble in order to evaluate its impact on the quality of data assimilation analysis. Results in Figure 11 show that the posterior RMSDs are reduced against those with the original experiments (Figures 2b and 4), especially during the storm main phase. The maximum value of prior RMSDs during the storm main phase is also reduced by 1 TECU (8 TECU down from 9 TECU for the 60 min cycling case; 7 TECU down from 8.5 TECU for the 30 min cycling case). The improvement is not clear for the shorter assimilation-forecast cycling case (10 min) in comparison to the original experiment. This suggests that the 10 min assimilation-forecast cycling leads to a better storm time ionospheric forecast than the 60 and 30 min cycling when the model ensemble is inconsistent with the realistic conditons. In other words, the way the model ensemble is generated does not affect the results of 10 min cycling case but becomes critical in the 30 and 60 min cycling cases. However, even if realistic

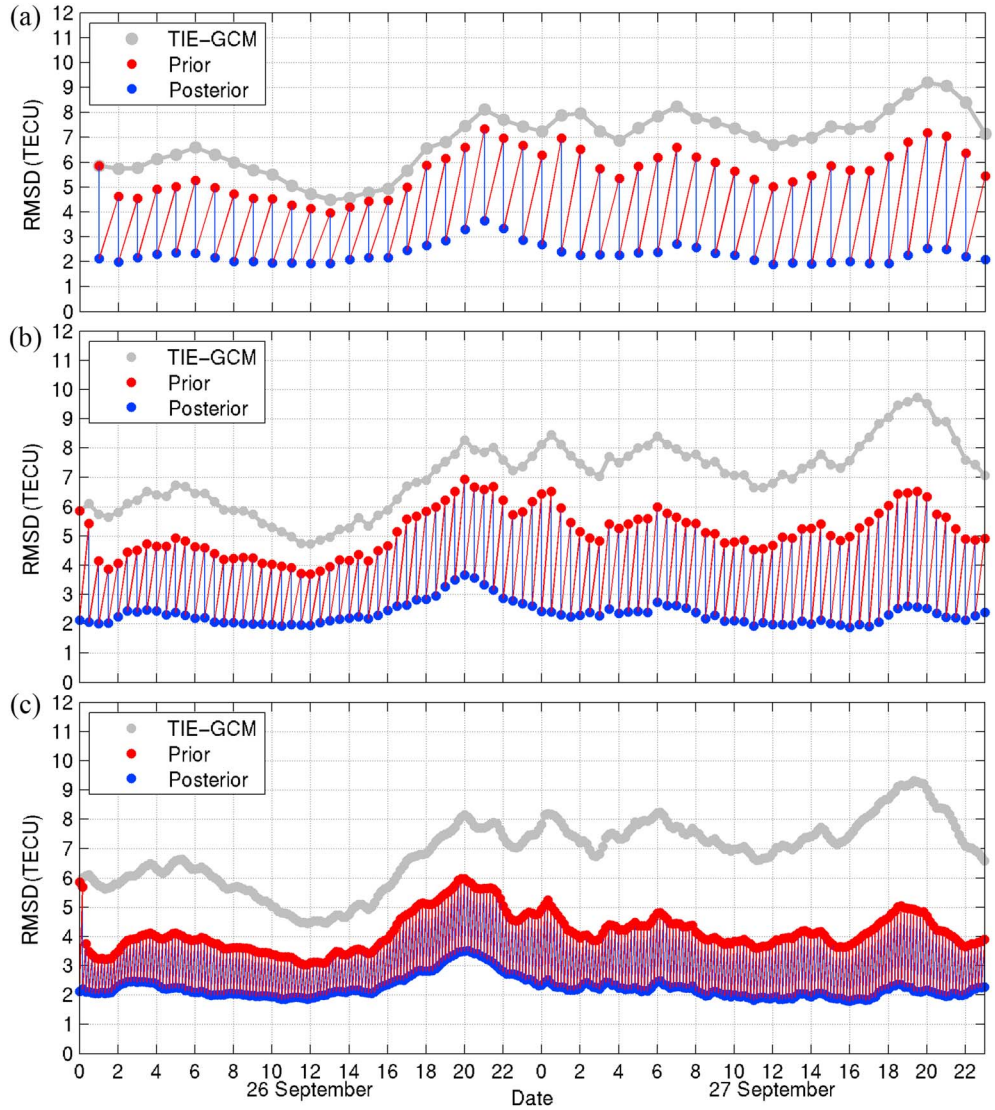

Figure 10. Time evolutions of RMSD in the cases of (a) 60, (b) 30, and (c) 10 min assimilation cycles without updating neutral variables in the assimilation system.

variation of *Kp* index is employed, it does not mean that the forecast model could capture thermospheric drivers correctly. This can be explained by the fact that the larger RMSDs of the standalone TIE-GCM driven by the realistic *Kp* index. Impacts of the model ensemble selection on the quality of assimilation analysis need to be investigated further.

Unrealistic model error growth associated with dynamical imbalance might also be due to the fact the electric field is not estimated by assimilation of GPS-TEC observations. Although the TIE-GCM calculates the dynamo electric field, currents, and electrodynamic feedback on neutral wind plasma motions, the data assimilation system does not directly adjust the electric field to be consistent with the updated state variables in the present astudy. Furthermore, the joule heating produced by magnetospheric currents and electric fields at auroral and subauroral latitudes during the geomagnetic storm period may not be appropriately specified in the TIE-GCM, which in turn results in unrealistic features of storm time neutral composition disturbances as represented by $\Sigma[O]/[N_2]$. It is possible that updated state variables reflect the impact of the storm time penetration electric fields on the thermosphere and ionosphere. Ideally, the estimation of these external drivers needs to be included in the ionospheric data assimilation system to improve the capability of forecasting during the geomagnetic storm time.

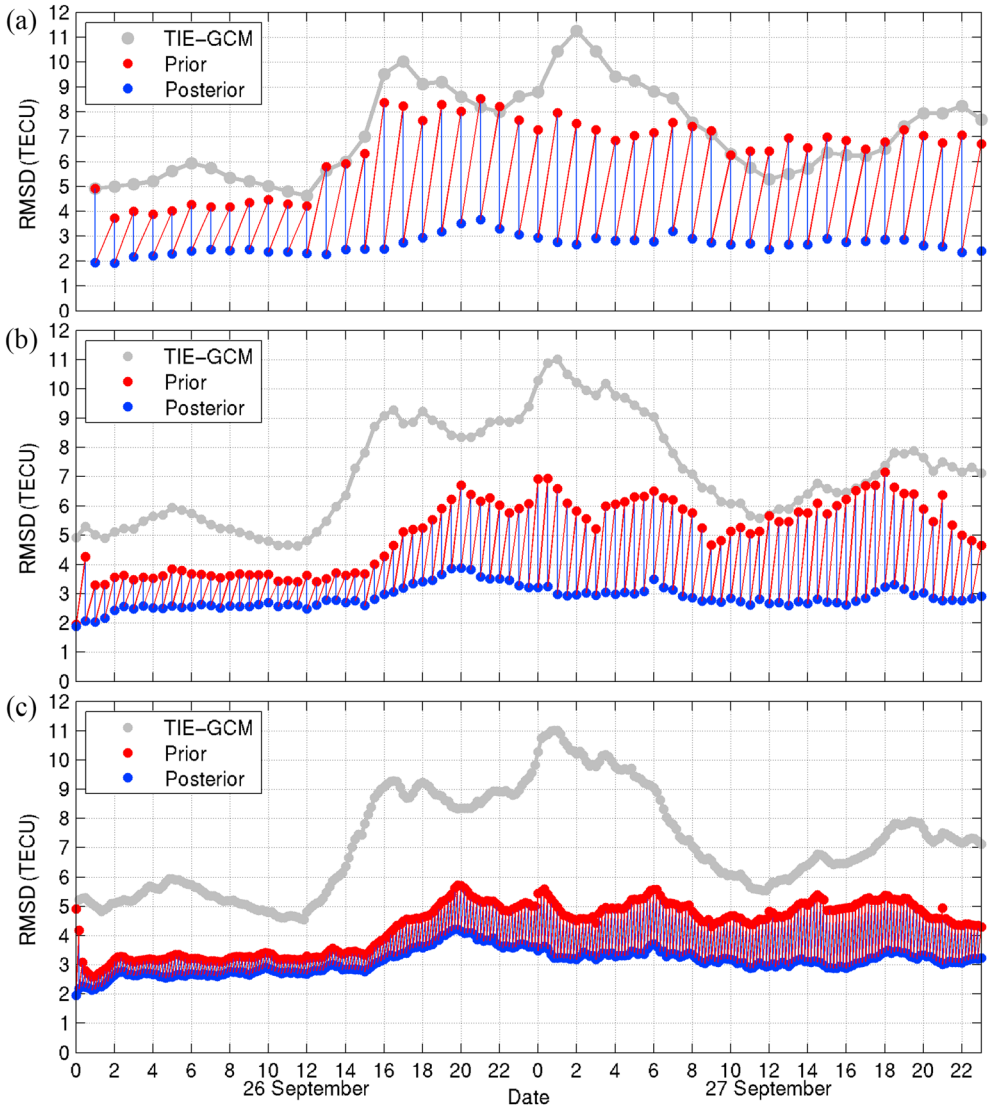

Figure 11. Time evolutions of prior RMSD with the realistic variation of *Kp* index by different assimilation cycles, (a) 60, (b) 30, and (c) 10 min, respectively.

4. Conclusions

An ionospheric data assimilation system is developed using the DART/TIE-GCM for global ground-based GPS-TEC observations in the present paper, and its capability to forecast ionospheric electron density is carefully evaluated for the geomagnetic storm on 26 September in 2011. In comparison to 60 and 30 min assimilation-forecast cycling, a shorter cycling (10 min in this study) greatly improves the fit to observations during the forecast (prior) stage of EnKF assimilation process (Figures 2b and 4). The result suggests that the EnKF assimilation system with shorter assimilation-forecast cycling may lead to better accuracy in the model forecast of ionospheric electron density during the geomagnetic storm even in the presence of forecast model biases. An assimilation experiment updating only ionospheric state variables, such as electron density and O^+ density, is further performed to evaluate effects of estimating unobserved neutral states on storm time forecasting. Results show that updating neutral state variables in the forecast model may be essential to enable the GPS-TEC observations to affect the model forecast dynamics. In the future work, all the relevant TIE-GCM model states and external drivers need to be made consistent to each other in the assimilation update which will likely further improve nowcasting and forecasting of the ionosphere during geomagnetic storm conditions.

Acknowledgments
This paper is supported by Ministry of Science and Technology (MOST) and National Space Organization (NSPO) of Taiwan to National Cheng Kung University under MOST-103-2111-M-006-001-MY2 and NSPO-S-102132. T.M. is supported by NASA award NNX14AI17G and AFOSR award FA9550-13-1-0058. The source code for the assimilation system and simulation model used in this study, the DART and TIE-GCM, are available at http://www.image.ucar.edu/DAReS/DART/ and http://www.hao.ucar.edu/modeling/tgcm/, respectively. The observations data from ground-based GPS receivers and TIMED-GUVI satellite are available at IGS (https://igscb.jpl.nasa.gov/components/data.html) and GUVI website (http://guvi.jhuapl.edu/levels/level3/guvi_on2/plot/gif/2011/ON2_2011_269.png). The GUVI data used here are provided through support from the NASA MO&DA program. The GUVI instrument was designed and built by the Aerospace Corporation and the Johns Hopkins University. The Principal Investigator is Andrew B. Christensen and the Chief Scientist and co-PI is Larry J. Paxton. The authors are grateful for the NCAR High Altitude Observatory and Data Assimilation Research Section for their support of TIE-GCM and DART software and thank the reviewers for their helpful comments.

References

Anderson, J. L., T. Hoar, K. Raeder, H. Liu, N. Collins, R. Torn, and A. F. Arellano (2009), The data assimilation research testbed: A community data assimilation facility, *Bull. Am. Meteorol. Soc.*, *90*, 1283–1296, doi:10.1175/2009BAMS2618.1.

Baumgardner, J., et al. (2013), Imaging space weather over Europe, *Space Weather*, *11*, 69–78, doi:10.1002/swe.20027.

Bhuiyan, M. Z. H. (2011), Analysis of multipath mitigation techniques for satellite-based positioning applications, PhD thesis, Dep. of Communications Engineering, Tampere University of Technology, Tampere, Finland.

Boyle, C. B., P. H. Reiff, and M. R. Hairston (1997), Empirical polar cap potentials, *J. Geophys. Res.*, *102*, 111–125, doi:10.1029/96JA01742.

Burns, A. G., T. L. Killeen, G. R. Carignan, and R. G. Roble (1995), Large enhancements in the O/N_2 ratio in the evening sector of the winter hemisphere during geomagnetic storms, *J. Geophys. Res.*, *100*, 14,661–14,671, doi:10.1029/94JA03235.

Chartier, A. T., D. R. Jackson, and C. N. Mitchell (2013), A comparison of the effects of initializing different thermosphere-ionosphere model fields on storm time plasma density forecasts, *J. Geophys. Res. Space Physics*, *118*, 7329–7337, doi:10.1002/2013JA019034.

Chartier, A. T., T. Matsuo, J. L. Anderson, N. Collins, T. J. Hoar, G. Lu, C. N. Mitchell, A. J. Coster, L. J. Paxton, and G. S. Bust (2016), Ionospheric data assimilation and forecasting during storms, *J. Geophys. Res Space Physics*, *121*, 764–778, doi:10.1002/2014JA020799.

Coster, A. J., M. J. Colerico, J. C. Foster, W. Rideout, and F. J. Rich (2007), Longitude sector comparisons of storm enhanced density, *Geophys. Res. Lett.*, *34*, L18105, doi:10.1029/2007GL030682.

Datta-Barua, S., G. S. Bust, and G. Crowley (2013), First storm time plasma velocity estimates from high-resolution ionospheric data assimilation, *J. Geophys. Res. Space Physics*, *118*, 7458–7471, doi:10.1002/2013JA019153.

Foster, J. C., and W. Rideout (2007), Storm enhanced density: Magnetic conjugacy effects, *Ann. Geophys.*, *25*(8), 1791–1799.

Foster, J. C., P. J. Erickson, A. J. Coster, J. Goldstein, and F. J. Rich (2002), Ionospheric signatures of plasmaspheric tails, *Geophys. Res. Lett.*, *29*(13), 1623, doi:10.1029/2002GL015067.

Fuller-Rowell, T. J., M. V. Codrescu, R. G. Roble, and A. D. Richmond (1998), How does the thermosphere and ionosphere react to a geomagnetic storm?, in edited by B. T. Tsurutani, W. D. Gonzales, and Y. Kamide, *Magnetic Storms, 240*, AGU Monograph, Washington, D. C.

Hajj, G. A., B. D. Wilson, C. Wang, X. Pi, and I. G. Rosen (2004), Data assimilation of ground GPS total electron content in to a physics-based ionospheric model by use of the Kalman filter, *Radio Sci.*, *39*, RS1S05, doi:10.1029/2002RS002859.

Heelis, R. A., J. K. Lowell, and R. W. Spiro (1982), A model of the high-latitude ionospheric convection pattern, *J. Geophys. Res.*, *87*(A8), 6339–6345.

Hsu, C.-T., T. Matsuo, W. Wang, and J.-Y. Liu (2014), Effects of inferring unobserved thermospheric and ionospheric state variables by using an Ensemble Kalman Filter on global ionospheric specification and forecasting, *J. Geophys. Res. Space Physics*, *119*, 9256–9267, doi:10.1002/2014JA020390.

Khattatov, B., M. Murphy, M. Gnedin, B. Cruickshank, J. Adams, V. Yudin, and T. Fuller-Rowell (2004), An ionospheric forecasting system, paper presented at Institute of Navigation Annual Technical Meeting, Long Beach, Calif., Sept.

Khattatov, B., M. Gnedin, M. Murphy, B. Cruickshank, J. Adams, V. Yudin, T. Fuller-Rowell, J. W. Wright, N. A. Zabotin, and M. J. Angling (2005), An AFRL sponsored ionospheric specification system, in edited by J. M. Goodman, *Proceedings of the 11th Ionospheric Effects Symposium*, pp. 501–511, Off. Of Nav. Res., Arlington, VA.

Lee, I. T., T. Matsuo, A. D. Richmond, J. Y. Liu, W. Wang, C. H. Lin, J. L. Anderson, and M. Q. Chen (2012), Assimilation of FORMOSAT-3/COSMIC electron density profiles into a coupled thermosphere/ionosphere model using ensemble Kalman filtering, *J. Geophys. Res.*, *117*, A10318, doi:10.1029/2012JA017700.

Lee, I. T., H. F. Tsai, J. Y. Liu, C. H. Lin, T. Matsuo, and L. C. Chang (2013), Modeling impact of FORMOSAT-7/COSMIC-2 mission on ionospheric space weather monitoring, *J. Geophys. Res. Space Physics*, *118*, 6518–6523, doi:10.1002/jgra.50538.

Liu, J. Y., H. F. Tsai, and T. K. Jung (1996), Total electron content obtained by using the Global Positioning System, *Terr. Atmos. Oceanic Sci.*, *7*, 107–117.

Lu, G., L. P. Goncharenko, A. D. Richmond, R. G. Roble, and N. Aponte (2008), A dayside ionospheric positive storm phase driven by neutral winds, *J. Geophys. Res.*, *113*, A08304, doi:10.1029/2007JA012895.

Matsuo, T., and E. A. Araujo-Pradere (2011), Role of thermosphere-ionosphere coupling in a global ionospheric specification, *Radio Sci.*, *46*, RS0D23, doi:10.1029/2010RS004576.

Meier, R., G. Crowley, D. J. Strickland, A. B. Christensen, L. J. Paxton, D. Morrison, and C. L. Hackert (2005), First look at the 20 November 2003 super storm with TIMED/GUVI: Comparisons with a thermospheric global circulation model, *J. Geophys. Res.*, *110*, A09S41, doi:10.1029/2004JA010990.

Pi, X., G. A. Hajj, B. D. Wilson, A. J. Mannucci, A. Komjathy, L. Mandrake, C. Wang, and I. G. Rosen (2004), Three-dimensional assimilative ionospheric modeling for regions of large TEC gradient, paper presented at National Technical Meeting, Inst. Of Navig., San Diego, Jan.

Richmond, A. D., E. C. Ridley, and R. G. Roble (1992), A thermosphere/ionosphere general circulation model with coupled electrodynamics, *Geophys. Res. Lett.*, *19*, 601–604, doi:10.1029/92GL00401.

Roble, R. G., E. C. Ridley, A. D. Richmond, and R. E. Dickinson (1988), A coupled thermosphere/ionosphere general circulation model, *Geophys. Res. Lett.*, *15*, 1325–1328, doi:10.1029/GL015i012p01325.

Sardon, E., A. Rius, and N. Zarraoa (1994), Estimation of the transmitter and receiver differential biases and the ionospheric total electron content from Global Positioning System observations, *Radio Sci.*, *29*, 577–586, doi:10.1029/94RS00449.

Scherliess, L., R. W. Schunk, J. J. Sojka, and D. C. Thompson (2004), Development of a physics-based reduced state Kalman filter for the ionosphere, *Radio Sci.*, *39*, RS1S04, doi:10.1029/2002RS002797.

Scherliess, L., R. W. Schunk, J. J. Sojka, D. C. Thompson, and L. Zhu (2006), Utah State University global assimilation of ionospheric measurements Gauss-Markov Kalman filter model of the ionosphere: Model description and validation, *J. Geophys. Res.*, *111*, A11315, doi:10.1029/2006JA011712.

Schunk, R. W., et al. (2004), Global Assimilation of Ionospheric Measurements (GAIM), *Radio Sci.*, *39*, RS1S02, doi:10.1029/2002RS002794.

Schunk, R. W., L. Scherliess, J. Sojka, D. Thompson, and L. Zhu (2005), Ionospheric weather forecasting on the horizon, *Space Weather*, *3*, S08007, doi:10.1029/2004SW000138.

Sojka, J. J., D. C. Thompson, L. Scherliess, R. W. Schunk, and T. J. Harris (2007), Assessing models for ionospheric weather specifications over Australia during the 2004 Climate and Weather of the Sun-Earth-System (CAWSES) campaign, *J. Geophys. Res.*, *112*, A09306, doi:10.1029/2006JA012048.

Solomentsev, D., K. S. Jacobsen, B. Khattatov, V. Khattatov, Y. Cherniak, and A. Titov (2014), Ionosphere data assimilation capabilities for representing the high-latitude geomagnetic storm event in September 2011, *J. Geophys. Res. Space Physics*, *119*, 581–10,594, doi:10.1002/2014JA020248.

Strickland, D. J., J. S. Evans, and L. J. Paxton (1995), Satellite remote sensing of thermospheric O/N_2 and solar EUV, *J. Geophys. Res.*, *100*, 12,217–12,226, doi:10.1029/95JA00574.

Thomas, E. G., J. B. H. Baker, J. M. Ruohoniemi, L. B. N. Clausen, A. J. Coster, J. C. Foster, and P. J. Erickson (2013), Direct observations of the role of convection electric field in the formation of a polar tongue of ionization from storm enhanced density, *J. Geophys. Res. Space Physics*, *118*, 1180–1189, doi:10.1002/jgra.50116.

Thompson, D. C., L. Scherliess, J. J. Sojka, and R. W. Schunk (2006), The Utah State University Gauss-Markov Kalman filter of the ionosphere: The effect of slant TEC and electron density profile data on model fidelity, *J. Atmos. Sol. Terr. Phys.*, *68*, 947–958.

Wang, C., G. Hajj, X. Pi, I. G. Rosen, and B. Wilson (2004), Development of the Global Assimilative Ionospheric Model, *Radio Sci.*, *39*, RS1S06, doi:10.1029/2002RS002854.

Wang, C., Q. Zhang, P. J. Chi, and C. Li (2013), Simultaneous observations of plasmaspheric and ionospheric variations during magnetic storms in 2011: First result from Chinese Meridian Project, *J. Geophys. Res. Space Physics*, *118*, 99–104, doi:10.1029/2012JA017967.

Wilson, D. B., A. J. Mannucci, C. D. Edwards, and T. Roth (1992), Global ionospheric maps using a global network of GPS receivers, the Int. Beacon Satellite Symposium, MIT, Cambridge, Mass., July 6-12.

Zhang, Y., and L. J. Paxton (2008), An empirical *Kp*-dependent global auroral model based on TIMED/GUVI FUV data, *J. Atmos. Sol. Terr. Phys.*, *70*, 1231–1242, doi:10.1016/j.jastp.2008.03.008.